Pramana – J. Phys. (2018) 90:77
https://doi.org/10.1007/s12043-018-1566-5

Apodization of two-dimensional pupils with aberrations

ANDRA NARESH KUMAR REDDY[1,3,4,*], MAHDIEH HASHEMI[2] and SVETLANA NIKOLAEVNA KHONINA[1,3]

[1]Samara National Research University, Moskovskoye Shosse, 34, Samara 443086, Russia
[2]Department of Physics, College of Science, Fasa University, Fasa 74617-81189, Iran
[3]Image Processing Systems Institute – Branch of the Federal Scientific Research Centre, "Crystallography and Photonics" of Russian Academy of Sciences, 151 Molodogvardeyskaya St., Samara 443001, Russia
[4]School of Engineering, Anurag Group of Institutions, Venkatapur, Ghatekesar, Medchal District, Hyderabad 500 088, India
*Corresponding author. E-mail: naarereddy@ssau.ru; naarereddy@gmail.com

MS received 30 August 2017; revised 4 December 2017; accepted 18 December 2017;
published online 11 May 2018

Abstract. The technique proposed to enhance the resolution of the point spread function (PSF) of an optical system underneath defocussing and spherical aberrations. The method of approach is based on the amplitude and phase masking in a ring aperture for modifying the light intensity distribution in the Gaussian focal plane ($Y_D = 0$) and in the defocussed planes ($Y_D = \pi$ and $Y_D = 2\pi$). The width of the annulus modifies the distribution of the light intensity in the side lobes of the resultant PSF. In the presence of an asymmetry in the phase of the annulus, the Hanning amplitude apodizer [$\cos(\pi\beta\rho)$] employed in the pupil function can modify the spatial distribution of light in the maximum defocussed plane ($Y_D = 2\pi$), results in PSF with improved resolution.

Keywords. Aberrations; diffraction; point spread function; apodization; resolution.

PACS Nos 42.15.Fr; 42.25.FX; 42.30.Kq

1. Introduction

The spatial distribution of the electromagnetic wave in the focal region can be controlled by using shaded or shaped apertures. Light distribution in the focal region of the optical system is determined by the transmission of light through the pupil function, which can be set to achieve the desired resolution and suppressed side lobes. By employing phase filters of different schemes, there were a number of studies that consider the possibility of improving the axial and lateral resolution of the PSF produced by the optical system [1–5]. Recently, the phase filters had drawn more attention than the amplitude filters for changing the size of the focal spot, i.e. the spatial redistribution of the light flux in the focal spot [6–10]. For instance, the pupil filters using Toraldo concept were used for apodizing the point spread function (PSF) in the transverse direction and succeeded to improve the resolution of the transverse PSF [11,12]. Similarly, the multiple annuli coded phase pupils were investigated to modify zero positions and intensities of the maxima and minima of the PSF in the image plane [13]. However, the amplitude filters were proved to be effective in the case of two-point imaging studies, i.e. detecting the image of an object which was hidden in the diffracted field of the neighbouring object [14,15]. Such filters were also used to apodize the optical system under the influence of defocussing [16,17]. For improving the resolution of the optical system, the phase pupil filters were presented with optimum performance [18,19] and these studies concluded that the phase filters can achieve the PSF with the side lobes much lower than the Airy ones with narrower central peak. A similar technique was used to achieve axial and lateral resolutions in the confocal scanning systems [20] and also applicable in exploring the extra solar planets [21]. On the other hand, the one-dimensional amplitude and phase filters were successful in modifying the positions and intensities of the minima and maxima of the PSF [22] and continued to quantify the image quality criteria such as the FWHM, HWHM of the PSF [23]. Even the one-dimensional amplitude and phase pupils were proved as an effective filter to improve the imaging performance of the optical system under the primary spherical aberration [24].

Principally, the suggested two-dimensional mask filters which can correct the PSF of the optical system in the presence of primary wave aberrations in the form of ring apertures or coded annular apertures are discussed in [13,18,19,25,26]. Here, we introduced the amplitude and phase apodization together in the pupil plane of the optical system and it shows that while the resolution of the optical system degrades in the presence of primary wave aberrations, it can be improved with the proposed annular masks. Modifying the maxima and minima positions and narrowing the central peak of the PSF are technically possible by employing the proposed mask filters. The defocussing effect shifts the focal spot longitudinally from the expected Gaussian point and causes the light flux to spread out from the central maximum to the side lobes. To correct such lens imperfection and also spherical aberration, we proposed filters in the form of ring apertures. In this article, filtering the high frequency responses of the PSF leading to the reduced side lobes are considered as 'apodization', while enhancement of high frequency response which concomitantly reduces the FWHM of PSF is considered as 'super-resolution'.

$$\text{Annular mask} = \begin{cases} \text{Left annulus, } -i = \mathrm{e}^{-i\pi/2}; & -\pi/2 \le \varphi \le \pi/2 \\ \text{Hanning amplitude mask } [\cos(\pi\beta\rho)]; & 0 \le \varphi \le 2\pi \\ \text{Right annulus, } +i = \mathrm{e}^{i\pi/2}; & \pi/2 \le \varphi \le 3\pi/2 \end{cases} \quad (1)$$

The annulus width (b) and the shading parameter (β) in the central circular region of the pupil filter together are capable of controlling the side-lobe intensities to achieve the PSF with enhanced resolution. The PSF distribution in the transverse and axial directions is modified by controlling the phase and amplitude simultaneously in the pupil plane. The pupil mask filters are very useful for achieving side-lobe suppression in the resultant intensity distribution of the PSF in the Gaussian focal plane ($Y_D = 0$) and the defocussed planes ($Y_D = \pi$ and $Y_D = 2\pi$). This work has reported various amounts of primary spherical wave aberration (Y_S). The optical system with the proposed apertures is linear and shift-variant. The resultant field which is produced by the aberrated aperture system is the convolution operation of the PSF.

2. Design and mathematical formulation

From the Fresnel-diffraction scalar wave theory, the PSF distribution in the focal region of the optical system is the Fourier transform of the pupil function. In this work, the analytical expression of the two-dimensional annular mask is introduced in eq. (1). The general scheme of the annular mask is illustrated in figure 1 which illustrates the schematic design of the proposed annular mask filters. The annulus is divided into two equal halves with the opposite phases and these two semicircular rings have uniform width of b (black and white shaded regions in figure 1). The central circular region of the annular aperture is subjected to a Hanning amplitude mask. ρ is the radial coordinate in the pupil, while β is the controlling parameter of the apodization in the central circular region of the annular mask. Here, the transmitted amplitude of the pupil also depends strongly on the annulus width b.

The complex amplitude distribution of the field of eq. (1), would be eq. (2) as follows:

$$\begin{aligned} A(u,\phi) &= -i\int_{1-b}^{1}\int_{-\pi/2}^{\pi/2} \exp(iu\rho\cos(\phi-\varphi))\rho\mathrm{d}\rho\,\mathrm{d}\varphi \\ &+ \int_{0}^{1-b}\int_{0}^{2\pi} \cos(\pi\beta\rho)\exp\left[-i\left(\frac{Y_D\rho^2}{2}+\frac{Y_S\rho^4}{4}\right)\right] \\ &\times \exp(iu\rho\cos(\phi-\varphi))\rho\mathrm{d}\rho\,\mathrm{d}\varphi \\ &+ i\int_{1-b}^{1}\int_{\pi/2}^{3\pi/2} \exp(iu\rho\cos(\phi-\varphi))\rho\,\mathrm{d}\rho\,\mathrm{d}\varphi, \end{aligned} \quad (2)$$

where $u = k\sin\theta = (2\pi/\lambda)\sin\theta$, λ is the wavelength of the incident beam of radiation and u is the dimensionless diffraction coordinate in the receiver plane of the optical system. Here, θ is the angle of orientation. $\cos(\pi\beta\rho)$ is the Hanning amplitude mask in the central circular zone (blue shaded region in figure 1) of the

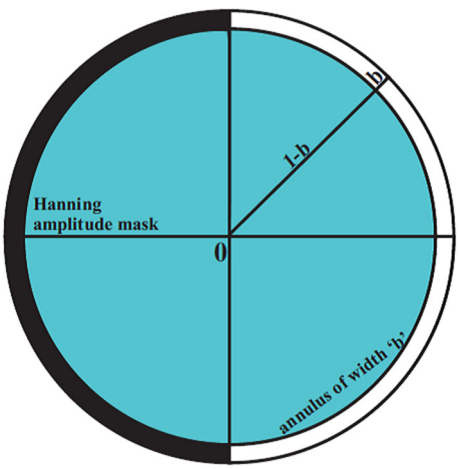

Figure 1. General scheme of the annular mask.

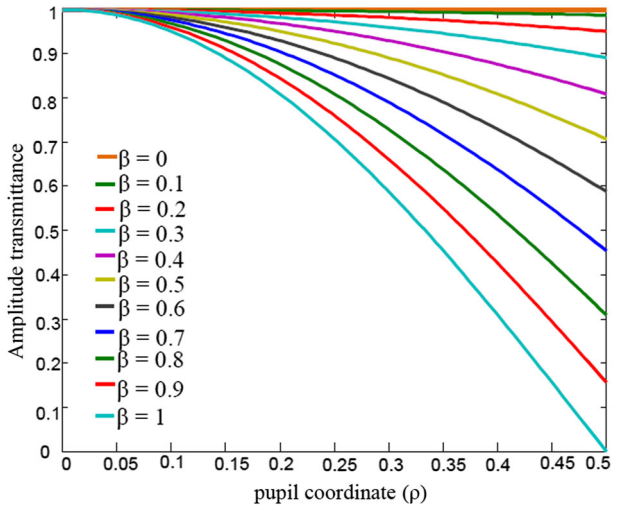

Figure 2. Amplitude transmittance of the Hanning amplitude apodizer for different values of β.

proposed filter. Here, Y_D and Y_S are the defocussing effect and the primary spherical aberration control parameters, respectively. For different Hanning amplitude apodizers, figure 2 illustrates a monotonic decrease of the amplitude transmittance of the central circular region with the radial coordinate ρ of the lens aperture. At the centre of the pupil, the transmittance is set to be maximised. For higher values of β, the transmittance decreases and approaches minimum. Optimised transmission is achieved when $\beta \to 1$. In the surrounding ring, we consider two complex conjugated phase elements with uniform amplitude transmittance. When filtering takes place in the right-hand side of the PSF, the square of the minimum intensity in the side-lobe region is used to determine the width of the annulus (b). The pupil function is employed in the form of antiphase functions which can modify intensity distribution in the diffraction field of the optical system. The parameter b is also known as the controlling parameter of the antiphase masking at the periphery of the lens aperture. The intensity PSF of the focal spot, which is a real and measurable quantity, is given by eq. (3):

$$I(u, \phi) = |A(u, \phi)|^2 . \tag{3}$$

The investigations of the results have been carried out using eq. (3), which is useful to compute the side-lobe levels and the central peak width of the PSF.

3. Results and discussion

To investigate the effect of defocussing and primary spherical aberration on the light intensity distributions as a function of diffraction coordinate u which is varied from -12 to $+12$, we employed the Gaussian quadrature method of numerical integration [27]. The method developed is an efficient and accurate method to investigate the positions and the intensities of the central peak, first minima and the first side lobes, while higher-order maxima and minima are neglected. The efficiency of the mask can be determined based on the intensity of the first side lobes, the width of the central peak and the positions of first minima in the PSF distribution. In this section, the mask efficiency is defined to investigate the optimum values of b and β. In this section, we investigate the central peak position and its full width and the intensity of lower order side lobe in the presence of various defocussing and spherical aberrations for different values of the annulus width around the Hanning amplitude apodizer in the pupil plane.

The computed values in table 1 explain that as the annulus width b increases from 0 to 0.094, the position of the central maxima shifts towards the left-hand side of the diffraction pattern in the Gaussian focal plane. In the Airy distribution ($\beta = 0$ and $b = 0$), as the amount of spherical aberration increases, the first minimum position shifts away from the diffracted peak and the first side-lobe intensity increases. For $b = 0.04$, for given values of Y_S, the first side-lobe intensity on the right-hand side of the main peak is obtained as near zero values of 0.0027, 0.0031 and 0.0085. In this case, the first side lobe is suppressed on the right-hand side, which is much flatter than the non-apodized ones (0.0174, 0.0186 and 0.0230). On the contrary, the first side-lobe intensity on the left-hand side increases. The first minimum position on the right-hand side shifts from $u = 4.4345$ to 6.6412 (u is the normalised dimensionless coordinate in the focal plane) and finally reaches $u = 6.4445$ whereas on the left-hand side the first minimum position shifts away from the central peak with the values of Y_S. For $b = 0.094$, in the presence of high spherical aberration ($Y_S = 2\pi$), the first minimum position is shifted closer to the central peak at $u = 3.7666$ whereas on the left-hand side the first minimum position is found at 3.8963. In this case, the central peak width (CPW) of the PSF is computed as 7.6629 whereas in the case of the Airy PSF ($\beta = 0$, $b = 0$ and $Y_S = 2\pi$), the CPW is 8.0614. It is clear that for the Gaussian focal plane ($Y_D = 0$), the presence of high spherical aberration causes the central peak width to decrease, which is less than that of the unapodized one. It is also observed that for $b = 0.094$, for given values of Y_S, the first side lobe on the right-hand side of the PSF distribution is found with low intensity. However, it is obtained at the cost of higher left-hand side lobe.

Table 1. Intensities and positions of maxima and minima of the PSF for the Gaussian focal plane ($Y_D = 0$).

β	b (annulus width)	Central maxima position			Central maxima intensity			First minima position (right side)			First secondary maxima intensity (right side)			First minima position (left side)			First secondary maxima intensity (left side)		
		$Y_S = 0$	π	$Y_S = 2\pi$	$Y_S = 0$	$Y_S = \pi$	$Y_S = 2\pi$	$Y_S = 0$	$Y_S = \pi$	$Y_S = 2\pi$	$Y_S = 0$	$Y_S = \pi$	$Y_S = 2\pi$	$Y_S = 0$	$Y_S = \pi$	$Y_S = 2\pi$	$Y_S = 0$	$Y_S = \pi$	$Y_S = 2\pi$
0	0	0	0	0	1	0.9464	0.8003	3.8317	3.8646	4.0307	0.01748	0.01865	0.02303	−3.8317	−3.8646	−4.0307	0.01749	0.01865	0.02303
	0.04	−0.3461	−0.3470	−0.3506	0.8743	0.8402	0.7449	4.4345	6.6412	6.4445	0.00271	0.00313	0.00858	−3.8192	−3.8396	−3.9101	0.03999	0.03906	0.03638
	0.094	−0.7930	−0.7970	−0.8101	0.7973	0.7780	0.7226	6.3010	6.3817	3.7666	0.01858	0.02075	0.02898	−3.8530	−3.8635	−3.8963	0.08033	0.07837	0.07278
1	0	0	0	0	0.16425	0.1661	0.16962	2.4551	2.4882	2.5853	0.06634	0.06215	0.05087	−2.4551	−2.4882	−2.5853	0.06634	0.06215	0.05087
	0.04	0.4913	0.4528	0.3294	0.1200	0.12026	0.12135	2.7050	2.7131	2.7386	0.09351	0.08910	0.07694	−2.0619	−2.1618	−2.4885	0.02827	0.02703	0.02392
	0.094	5.0029	5.0086	5.0264	0.13838	0.13481	0.12467	7.1225	7.1294	7.1503	0.05169	0.05021	0.04598	2.9799	2.9822	2.9893	0.10822	0.10547	0.09772

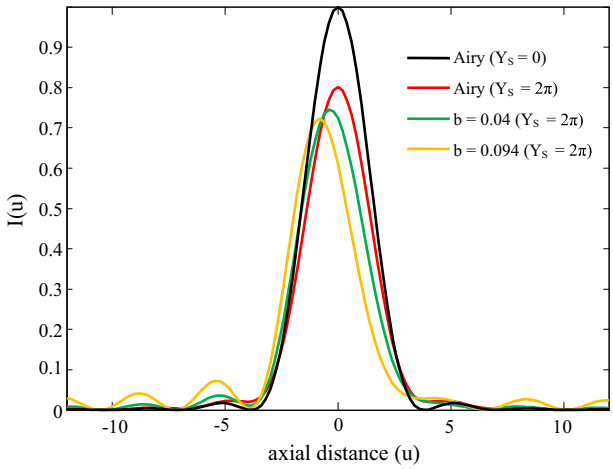

Figure 3. Unapodized and apodized PSF distributions in the presence of high spherical aberration for the Gaussian focal plane ($Y_D = 0$) when $\beta = 0$.

Figure 3 illustrates that in the presence of high spherical aberration ($Y_S = 2\pi$), a non-zero first minima is found on both sides of the Airy PSF of the Gaussian focal plane ($Y_D = 0$) whereas for the apodized PSFs ($b = 0.04$ and 0.094) the positions of the first minima have modified on both sides of the main peak, i.e. on the left-hand side of the PSF, the first minima approach zero intensity level.

It is also observed that the CPW of the Airy PSF for $Y_S = 0$ is computed as 7.6634 whereas the central peak width of the aberrated Airy PSF ($Y_S = 2\pi$) is 8.0614. CPW of the apodized PSFs for $b = 0.04$, 0.094 in the presence of high spherical aberration is computed as 10.3546 and 7.6629, respectively. It is concluded that by adjusting the annulus width (b) of the pupil to the optimum value, the resolution of the PSF in the axial direction is improved in the form of suppressed side lobes and the tailored central peak width.

On introducing the Hanning amplitude shade ($\cos(\pi\beta\rho)$, where $\beta \to 1$) in the central circular region of the lens aperture, the first minimum position on both sides of the central peak are adjusted to the required position. For $b = 0$, as the degree of the spherical aberration increases from 0 to 2π in steps of π, the first minimum position on the right side of the PSF shifts from $u = 2.4551$ to 2.5853 and the intensity of the first side lobe decreases from 0.06634 to 0.06215 and then reaches 0.05087 in the PSF distribution of the Gaussian focal plane. Similar trends are noticed for the first minimum positions in the defocussed planes, but the first side-lobe intensities in the defocussed plane ($Y_D = \pi$) are found to be lower than the first side-lobe intensity values found in the Gaussian focal plane. It is clear that

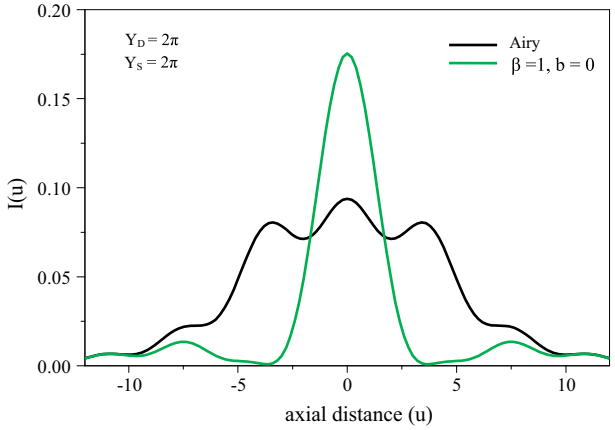

Figure 4. Variation in the axial distribution of the PSF under the combined influence of high defocussing and spherical aberrations.

the magnitude of the first side-lobe intensity depends on the amount of defocussing effect (Y_D).

From figure 4, it is observed that in the presence of high spherical aberration ($Y_S = 2\pi$), the central peak intensity produced by the circular Airy pupil is decreased in low value for the maximum defocussed plane ($Y_D = 2\pi$), i.e. the interior energy of the central peak to spread out into the side-lobe region, which causes the PSF to almost lose its axial shape with non-zero at first minima. As β increased from 0 to 1, the central peak has reshaped, the first minimum positions are adjusted to the zero level and there is a decrease in the size of the focal spot produced by the shading lens aperture as a result of redistributed PSF in the focal region. It is clear that by employing the circular shaded aperture ($\beta = 1$ and $b = 0$) (values are listed in tables 1 and 3), for given values of the primary spherical aberration, the intensities of the central peak found in the maximum defocussed plane ($Y_D = 2\pi$) are higher than that of the Gaussian focal plane ($Y_D = 0$). From the computed values in table 1, for $\beta = 1$, for all values of Y_S, as b increases from 0 to 0.04, the first side lobe on the left-hand side of the PSF has intensity values closer to the zero level.

From the values listed in table 2, it is observed that for the Airy case, as the value of Y_S increases from 0 to 2π, the first side-lobe intensity decreases from 0.03196 to 0.00812 and then reaches 0.01201 for the defocussed plane ($Y_D = \pi$). For $\beta = 0$, as the width of the annulus increases from 0 to 0.04, the first side lobe on the left-hand side is suppressed at the cost of the enhanced first side lobe on the right-hand side of the PSF, i.e. the magnitude of the side-lobe suppression has increased with the Y_S value. For the same value of

Table 2. Intensities and positions of the PSF maxima and minima for the defocussed plane ($Y_D = \pi$).

β	b (annulus width)	Central maxima position			Central maxima intensity			First minima position (right side)			First secondary maxima intensity (right side)			First minima position (left side)			First secondary maxima intensity (left side)		
		$Y_S = 0$	$Y_S = \pi$	$Y_S = 2\pi$	$Y_S = 0$	$Y_S = \pi$	$Y_S = 2\pi$	$Y_S = 0$	$Y_S = \pi$	$Y_S = 2\pi$	$Y_S = 0$	$Y_S = \pi$	$Y_S = 2\pi$	$Y_S = 0$	$Y_S = \pi$	$Y_S = 2\pi$	$Y_S = 0$	$Y_S = \pi$	$Y_S = 2\pi$
0	0	0	0	0	0.8105	0.6133	0.4026	3.8317	6.9435	6.8443	0.03196	0.00812	0.01201	−3.8317	−6.9435	6.8443	0.03196	0.00812	0.01201
	0.04	−0.2935	−0.2699	−0.2452	0.7254	0.5845	0.4274	3.8311	3.5337	3.2527	0.03093	0.05197	0.07159	−3.9098	−4.0884	−4.6499	0.03615	0.03244	0.02799
	0.094	−0.7626	−0.7693	−0.7998	0.6730	0.5770	0.4677	3.4066	3.2066	3.0639	0.04593	0.06824	0.09116	−3.9287	−4.0098	−4.1326	0.06403	0.05382	0.04289
1	0	0	0	0	0.1998	0.2093	0.2031	2.6604	2.8313	3.0389	0.04949	0.03458	0.02015	−2.6604	−2.8313	−3.0389	0.04949	0.03458	0.02015
	0.04	0.1616	−0.0911	−0.3206	0.1383	0.1511	0.1622	2.7496	2.8093	2.9097	0.06890	0.05058	0.03281	−2.8067	−3.1130	−3.2827	0.02551	0.02319	0.02049
	0.094	5.0337	5.0725	−1.0547	0.1114	0.09351	0.1262	7.1616	7.2062	3.0084	0.04053	0.03315	0.07485	2.9801	2.9905	−3.6408	0.09011	0.09156	0.02741

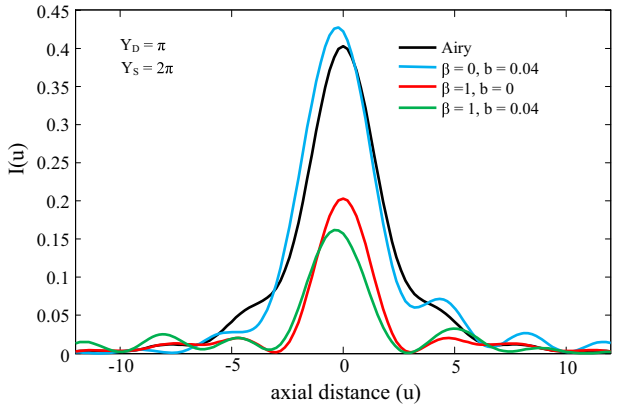

Figure 5. Tailoring the axial shape of the PSF under the influence of high spherical aberration in the defocussed plane for different masking conditions in the pupil plane.

b (0.04), the first minimum position on the right-hand side moves from $u = 3.8311$ to 3.2527 which is situated very close to the central peak of the corresponding PSF. In this case, the CPW for given values of the spherical aberration is computed as 7.7409, 7.6221 and 7.9026. The values obtained in this case are less than the values obtained for the Airy case in the defocussed plane ($Y_D = \pi$).

For $b = 0.094$ (as $\beta \to 0$), as the value of Y_S increases from 0 to 2π, the first minimum position on the right-hand side shifts from $u = 3.4066$ to 3.0639, whereas on the left-hand side, it moves from $u = 3.9287$ to 4.0098. Meanwhile, the first side-lobe suppression has been improved. In this case, the CPW of the PSF are 7.3353, 7.2164 and 7.1965.

Figure 5 illustrates the PSF distribution under the combined influence of the spherical aberration ($Y_S = 2\pi$) and the partial defocussing effect ($Y_D = \pi$). It is observed that for the Airy pupil, the image of the point object is longitudinally displaced and the interior energy of the central peak is displaced in the side-lobe region. In this case, the shape of the PSF is modulated by adjusting the annulus width (b) along with the value of β. For $b = 0.04$, the positions of non-zero first minima on both sides of the main peak have been modified and the amount of energy enclosed in the central disc has increased. For the apertures of $\beta = 1$ and $\beta = 1$, $b = 0.04$, the PSF distribution converts into the required component. In both cases, the side-lobe suppression has significantly improved and the first minimum position on both sides of the central maximum approaches the zero-level intensity. The CPW of the redistributed PSF in these cases are 6.0778 and 6.1924.

From the values listed in table 3, we can see that, in the Airy case for the maximum defocussed plane,

Table 3. Intensities and positions of maxima and minima of the PSF under the influence of spherical aberration for the defocussed plane ($Y_D = 2\pi$).

β	b (annulus width)	Central maxima position			Central maxima intensity			First minima position (right side)			First secondary maxima intensity (right side)			First minima position (left side)			First secondary maxima intensity (left side)		
		$Y_S = 0$	$Y_S = \pi$	$Y_S = 2\pi$	$Y_S = 0$	$Y_S = \pi$	$Y_S = 2\pi$	$Y_S = 0$	$Y_S = \pi$	$Y_S = 2\pi$	$Y_S = 0$	$Y_S = \pi$	$Y_S = 2\pi$	$Y_S = 0$	$Y_S = \pi$	$Y_S = 2\pi$	$Y_S = 0$	$Y_S = \pi$	$Y_S = 2\pi$
0	0	0	0	0	0.4053	0.2216	0.09404	3.5975	3.1694	2.0177	0.07211	0.08211	0.08057	−3.5975	−3.1694	−2.0177	0.07211	0.08211	0.08057
	0.04	−0.0696	0.0503	0.2500	0.39958	0.25607	0.14201	3.1263	2.9218	2.6953	0.08820	0.09922	0.10007	−8.0020	−8.6108	−5.7295	0.00034	0.00296	0.017586
	0.094	−0.5631	−0.4769	0.1199	0.39082	0.28386	0.19155	3.0873	3.0042	2.9326	0.11843	0.13623	0.14708	−4.2634	−4.4857	−4.7119	0.03062	0.02195	0.01589
1	0	0	0	0	0.24633	0.22105	0.17542	3.1105	3.3303	3.6714	0.01861	0.00843	0.01346	−3.1105	−3.3303	−3.6714	0.01861	0.00843	0.01346
	0.04	−0.4095	−0.5190	−0.6034	0.19680	0.19790	0.18210	2.9714	3.2167	3.7315	0.02299	0.01224	0.00809	−3.3275	−3.4182	−3.5177	0.02398	0.02044	0.01618
	0.094	−1.0600	−1.0875	−1.1171	0.16831	0.19348	0.20613	2.9759	2.9929	2.9923	0.05689	0.04241	0.03262	−3.5870	−3.5798	−3.5931	0.03811	0.04249	0.04412

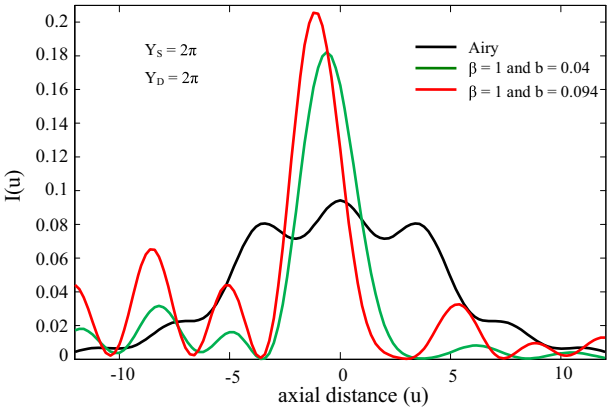

Figure 6. Intensity profile curves of the PSF in the presence of the highest degree of spherical and defocussing aberrations.

as the amount of the spherical aberration increases, the position of the first minimum shifts closer to the central peak. For $\beta = 0$ and $b = 0.04$, as the values of Y_S increase, the central peak initially shifts towards the left-hand side and then retraces back for the maximum spherical aberration. For given values of Y_S, the first side-lobe intensity on the left-hand side is found with almost zero-level intensity at the cost of increased first side lobe on the right side of the PSF. Similar trends are noticed for $b = 0.094$. By employing the circular shading mask ($\beta \neq 0$ and $b = 0$), as the amount of the spherical aberration increases, the first minimum position shifts away from the central peak and the first side-lobe intensity decreases from 0.01861 to 0.00843 and then reaches 0.01346. As the annulus width adjusts to 0.04, the central peak shifts away from the centre towards the left side of the pattern with the values of Y_S and the first side-lobe intensity on the right side decreases from 0.02299 to 0.00809 as the value of the first side-lobe intensity on the left side decreases from 0.02398 to 0.01618. From this study, it is concluded that in the presence of spherical aberration (Y_S), $Y_D = 2\pi$ is the best defocussed plane of the optical system with the proposed filters.

Figure 6 depicts the PSF distributions for different masking conditions in the pupil plane under the combined influence of high defocussing effect ($Y_D = 2\pi$) and high primary spherical aberration ($Y_S = 2\pi$). It is observed that for the unapodized case (Airy), the PSF has lost its axial resolution, resulting in a non-zero minima and enhanced side lobes. With apodized lens aperture ($\beta \to 1$ and $b = 0.04$), levels of the first minima on both sides of the main peak approach zero and the intensity of the lower- and higher-order side lobes on the right side of the PSF are suppressed. It is observed that the first dark region seen in the vicinity of the central peak is extended towards the right-hand side, which facilitates the detection of direct image of the low-intensity object in the proximity of the bright intensity object. This effect is very useful in astronomical and spectroscopic observations. On the contrary, the diffraction pattern on the left-hand side worsens as a price of obtaining the pattern on the right-hand side. The central peak width in this case is 7.2492, which is lower than that of the unapodized one, i.e. the width of the main peak with respect to the centre of the pattern on the right side is decreased at the cost of increased width on the left-hand side.

For the maximum defocussing ($Y_D = 2\pi$), using the annulus aperture of width $b = 0.094$, the central peak becomes narrower and the first minima on both sides are found with zero-level intensity. The first dark region found on the right side has extended to certain distance, which is helpful for resolving closely accompanied lines or objects with widely varying intensities. The central peak width in this case is 6.5854, and it is the optimum value obtained for the main peak produced by the lens aperture, relatively with the other apodized or unapodized cases.

4. Conclusions

It is concluded that for the Gaussian focal plane ($Y_D = 0$), the PSF with improved axial resolution has been produced by the optimal pupil function. The PSF in the Gaussian and defocussed planes is realised, with simultaneous suppression of the first side lobes and sharpening of the central peak is achieved on one side at the cost of deteriorating its counterpart. In the presence of spherical wave aberration, the first side lobe in the PSF distribution is found with zero-level intensity for the annulus width $b = 0.04$. For $b = 0.094$, the central peak width became much narrower than the Airy one, resulting in steep principal maxima, which are shifted towards the left-hand side of the pattern. The apodization efficiency of the aperture under the influence of defocussing and the primary spherical wave aberrations greatly depend on the values of b and β. The proposed filters are found to be more effective in the defocussed planes than in the Gaussian focal plane for redistribution of the light energy in the focal region. For the defocussed planes, by using optimum aperture, the resolution of the PSF in axial and transverse directions has been improved. This novel approach constitutes an effective step in designing real-time optical structures to enhance the resolving power of the imaging optics with optical aberrations, which can be applicable in confocal scanning systems and photonic structures for tight focussing of light.

Acknowledgements

This work was partially financially supported by Ministry of Education and Science of Russian Federation and Russian Foundation for Basic Research (RFBR) (16-29-11698, 16-29-11744).

References

[1] J P Mills and B J Thompson, Selected papers on apodization: Coherent optical systems, in: *SPIE milestone series* (SPIE Optical Engineering Press, Ellingham, 1996) Vol. MS 119
[2] P Jacquinot and B Roizen-Dossier, *Prog. Opt.* **3**, 29 (1964)
[3] R Barakat, *J. Opt. Soc. Am.* **52**, 276 (1962)
[4] R Barakat, *J. Opt. Soc. Am.* **52**, 264 (1962)
[5] S N Khonina and A V Ustinov, *Pattern Recogn. Image Anal.* **25(4)**, 626 (2015)
[6] T R M Sales and G M Morris, *Opt. Commun.* **156**, 227 (1998)
[7] S N Khonina, *Opt. Eng.* **52(9)**, 091711:1–6 (2013).
[8] W Yang and A B Kostinski, *J. Mod. Opt.* **52(17)**, 2467 (2005)
[9] M N Zervas and D Tarvener, *Fiber Integrat. Opt.* **19(4)**, 355 (2000)
[10] L N Hazra and N Reza, *Pramana – J. Phys.* **75**, 855 (2010)
[11] M Martinez-Corral, M T Caballero, E H K Stelzer and J Swoger, *Opt. Exp.* **10(1)**, 98 (2002)
[12] N Reza and L N Hazra, *J. Opt. Soc. Am. A* **30(2)**, 189 (2012)
[13] C Ratnam, V Lakshman Rao and S Lachaa Goud, *J. Phys. D* **39**, 4148 (2006)
[14] T Asakura and T Ueno, *Nouv. Rev. Opt.* **5**, 349 (1974)
[15] T Asakura, *Nouv. Rev. Opt.* **5**, 169 (1974)
[16] D Karuna Sagar, R Sayanna and S L Goud, *Opt. Commun.* **217**, 59 (2003)
[17] D Karuna Sagar, G Bikshamaiah, M Keshavulu Goud and S Lacha Goud, *J. Mod. Opt.* **53(14)**, 2011 (2006)
[18] L Cheng and G G Siu, *Meas. Sci. Technol.* **2(3)**, 198 (1991)
[19] G G Siu, L Cheng and D S Chiu, *J. Phys. D* **27(3)**, 459 (1994)
[20] M Kowalczyk, C J Zapata-Rodriguez and M Martinez-Corral, *Appl. Opt.* **37(35)**, 8206 (1998)
[21] W Yang and A B Kotinski, *Astrophys. J.* **605(2)**, 892 (2004)
[22] M K Goud, R Komala, A N K Reddy and S L Goud, *Acta Phys. Polon. A* **122(1)**, 90 (2012)
[23] A N K Reddy and D Karuna Sagar, *Pramana – J. Phys.* **84(1)**, 117 (2015)
[24] A N K Reddy and D Karuna Sagar, *Adv. Opt. Technol.* **2016**, 1 (2016)
[25] S C Biswas and A Boivin, *Opt. Acta* **23(7)**, 569 (1976)
[26] L N Hazra, P K Purkait and M De, *Can. J. Phys.* **57**, 1340 (1979)
[27] J H Mathews and K D Fink, *Numerical methods using Matlab* edited by Pearson, 4th edn (Prentice Hall Press, New Jersey, 2004) 4th edn